Tomographic phase microscopy

Wonshik Choi[1], Christopher Fang-Yen[1], Kamran Badizadegan[1,2], Seungeun Oh[1], Niyom Lue[1], Ramachandra R Dasari[1] & Michael S Feld[1]

We report a technique for quantitative three-dimensional (3D) mapping of refractive index in live cells and tissues using a phase-shifting laser interferometric microscope with variable illumination angle. We demonstrate tomographic imaging of cells and multicellular organisms, and time-dependent changes in cell structure. Our results will permit quantitative characterization of specimen-induced aberrations in high-resolution microscopy and have multiple applications in tissue light scattering.

High-resolution light microscopy is limited not only by the diffraction properties of light but also the optical inhomogeneities of the sample. Adaptive optics[1] and deconvolution techniques[2] can be used to correct sample-induced aberrations if the aberrations resulting from the refractive index variations are adequately measured. To be most effective, however, both correction strategies require quantitative knowledge of the 3D position-dependent refractive index of the sample.

The refractive index reveals a unique aspect of cellular structure, and is important in studies of cell and tissue light scattering, laser trapping of single cells, flow cytometry, total internal reflection microscopy and other areas involving the interaction of light with cells and tissues.

Classical methods for cellular index measurement provide only the average refractive index of a cell, ignoring spatial variations owing to subcellular structure. Moreover, they require immersion of cells in liquids of various refractive indices and subsequent observation with phase contrast microscopy[3]. This procedure is cumbersome and is limited by the tendency of some cells to be altered by the immersion liquids, which are typically not physiologically controlled. More recently, accurate measurements of average refractive index have been performed using microscopy techniques[4,5], which quantitatively measure optical phase shifts induced by the sample, but measurement of 3D spatial variation is still not possible.

One strategy for 3D determination of refractive index is based on measurement of projections of refractive index in multiple directions, in analogy to computed X-ray tomography, in which the projection of absorption is measured. Projections of refractive index have been performed via several quantitative phase microscopy techniques[4,6,7], and two earlier studies have used beam rotation[8] or sample rotation[9] to form tomographic images. But in one case quantitative refractive index information had not been provided[8], and the other required glycerol immersion of the sample and physical rotation of the sample in a micropipette[9].

We present a technique for quantitative, high-resolution 3D refractive index measurements of suspended or substrate-attached cells and multicellular organisms with no need for sample perturbation or immersion in special media. The setup (**Fig. 1**) is based on a Mach-Zehnder heterodyne interferometer[10], which provides quantitative phase images from time-dependent interference patterns induced by the frequency shifting of a reference beam relative to the sample beam. A helium-neon laser beam ($\lambda = 633$ nm) is divided into sample and reference arm paths by a beamsplitter. A galvanometer-mounted tilting mirror is used to vary the angle of illumination of the sample, which is positioned between the oil-immersion condenser and objective lenses. In the reference arm, the laser beam passes through two acousto-optic modulators (AOMs), which shift the frequency of the laser beam by 1,250 Hz. A second beamsplitter recombines the sample and reference laser beams, forming an interference pattern at the image plane. For each angle of illumination a complementary metal-oxide semiconductor (CMOS) camera (Photron 1024PCI) records

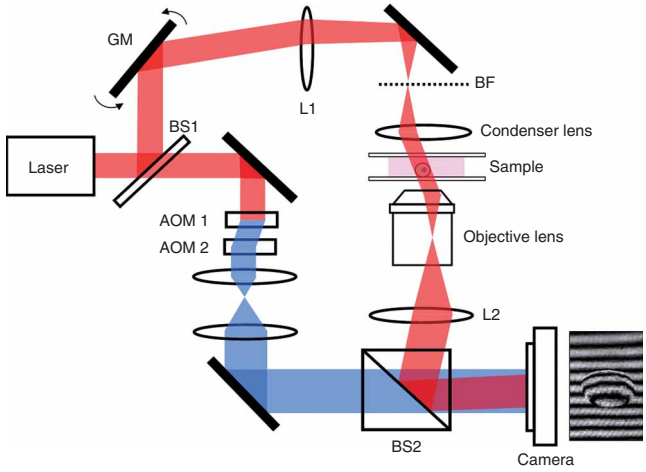

Figure 1 | Tomographic phase microscope. BS1 and BS2, beamsplitters 1 and 2; GM, galvanometer scanning mirror; L1, focal length $f = 250$-mm lens; BF, back focal plane of condenser lens; L2, $f = 200$-mm lens. The sample laser beam with original laser frequency is shown in red, and the frequency-shifted reference laser beam is shown in blue. A typical fringe pattern for a tilted beam illuminating a single HeLa cell is shown.

[1]G.R. Harrison Spectroscopy Laboratory, 77 Massachusetts Avenue 6-014, Massachusetts Institute of Technology, Cambridge, Massachusetts 02139, USA. [2]Department of Pathology, Harvard Medical School and Massachusetts General Hospital, Boston, Massachusetts 02114, USA. Correspondence should be addressed to M.S.F. (msfeld@mit.edu).

RECEIVED 30 MAY; ACCEPTED 6 JULY; PUBLISHED ONLINE 12 AUGUST 2007; DOI:10.1038/NMETH1078

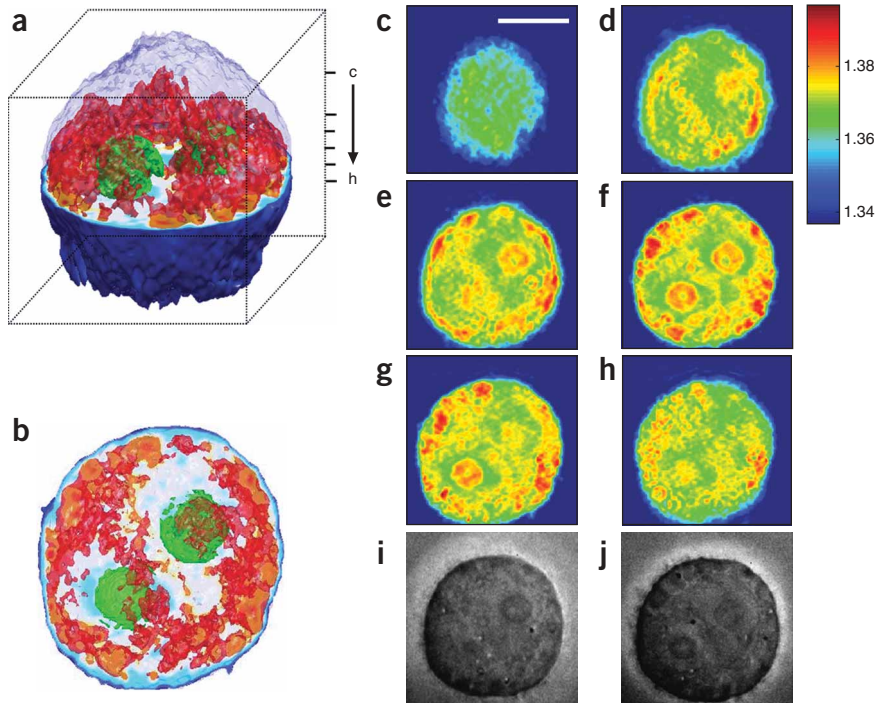

Figure 2 | Refractive index tomogram of a HeLa cell. (**a**) A 3D rendered image of a HeLa cell. The outermost layer of the upper hemisphere of the cell is omitted to visualize the inner structure. Nucleoli are colored green and parts of cytoplasm with refractive index higher than 1.36 are colored red. The side of the cube is 20 μm. (**b**) Top view of **a**. (**c**–**h**) Slices of the tomogram at heights indicated in **a**. Scale bar, 10 μm. Color bar, refractive index at $\lambda = 633$ nm. (**i**,**j**) Brightfield images for objective focus corresponding to **e** and **f**, respectively.

4 images at 5,000 frames/s, such that the sample-reference phase shift between consecutive frames is $\pi/2$. Phase images are then calculated by applying phase-shifting interferometry (**Supplementary Methods** online).

For near-plane wave illumination of a thin sample with small index contrast, the phase of the transmitted field is to a good approximation equal to the line integral of the refractive index along the path of beam propagation. Therefore, the phase image can simply be interpreted as the projection of refractive index, analogous to the projection of absorption in X-ray tomography (see **Supplementary Fig. 1** online for a diagram of the phase projection geometry).

To reconstruct a 3D refractive index tomogram from the projection phase images, we applied a procedure based on the filtered back-projection method[11]. We applied a discrete inverse Radon transform to every x-θ slice in the beam rotation direction, with x, the coordinate in the tilt direction and θ, the relative angle of sample laser beam direction to the optic axis of the objective lens. To compensate for the angle between imaging and illumination directions, we first divide the x values by $\cos\theta$. Illumination angles are limited to $|\theta| < 60^\circ$ by the numerical aperture of condenser and objective lenses. To reduce the effects of the missing projections, we applied an iterative constraint method (**Supplementary Methods** and **Supplementary Software 1** online).

To validate our instrument's measurements, we first measured refractive index tomograms of 10 μm polystyrene beads (Polysciences; $n = 1.588$ at $\lambda = 633$ nm) immersed in oil with a slightly lower refractive index (Cargille; $n = 1.559$ at $\lambda = 633$ nm). Tomograms showed a constant refractive index inside each bead, and the refractive index difference between the bead and its surroundings was $\Delta n = 0.0285 \pm 0.0005$, in agreement with the manufacturers' specifications for beads and oil ($\Delta n = 0.029$). Similar tests with a range of oil refractive indices from $n = 1.55$ to $n = 1.59$ also gave good agreement. By measuring the width (FWHM) of the derivative of line profiles of refractive index normal to the boundary of the sphere, we estimated the spatial resolution of our tomographic technique to be approximately 0.5 μm in the transverse (x-y) directions and 0.75 μm in the longitudinal (z) direction.

Next we imaged single HeLa cells in culture medium. We dissociated the cells from culture dishes and allowed them to partially attach to the coverslip substrate. Analysis of a 3D index tomogram for a single cell (**Fig. 2a**,**b** and **Supplementary Video 1** online) and x-y tomographic slices of the same cell at heights of $z = 12$, 9.5, 8.5, 7.5, 6.5 and 5.5 μm above the substrate (**Fig. 2c**–**h**) indicated that the index of refraction is highly inhomogeneous, varying from 1.36 to 1.40. There is a clear correspondence between the tomographic (**Fig. 2e**,**f**) and corresponding brightfield images (**Fig. 2i**,**j**) in terms of cell boundary, nuclear boundary as well as size and shape of the nucleoli.

Note that the refractive index of the nucleus ($n = 1.355$–1.365), apart from the nucleolus, is smaller than some parts of the cytoplasm ($n = 1.36$–1.39) and that the refractive index of the nucleoli, $n = 1.375$–1.385, is larger than that of the rest of the nucleus. This is contrary to the widely cited claims that the refractive index of the nucleus as a whole is higher than that of the rest of the cell[12]. We obtained similar results for cultured HEK 293 cells, B35 neuroblastoma cells and primary rat hippocampal neurons. All imaged cells contained many small cytoplasmic particles with high refractive index, which may be lipid droplets, lysosomes, vacuoles or other organelles.

We next used refractive index tomography to examine physiological changes in living cells. Whitening of areas of the cervix resulting from topically applied acetic acid is widely used to identify suspicious sites of precancerous lesions. It has been suggested that coagulation of nucleus protein may increase the refractive index contrast between nucleus and cytoplasm[13]. To investigate the effect of low concentrations of acetic acid on the structure of a cell and explain the mechanism of acetic acid whitening, we used our tomographic microscope to record index tomograms of HeLa cells after changing the cell environment from normal culture medium to culture medium containing 0.38% acetic acid (**Fig. 3a**,**b**). Tomograms could be obtained in less than 10 s, allowing measurements of relatively rapid changes in cell structure resulting from external perturbations. The refractive index of the nucleolus increased from 1.36 to 1.39, and the

inhomogeneity of the rest of the nucleus increased dramatically. This suggests that the increased scattering associated with acetal whitening results from both increased refractive index contrast between nucleoli and the rest of the cell, and increased heterogeneity of refractive index throughout the cell. Three minutes after replacing the acetic acid–containing medium with normal culture medium, the spatial variation and refractive index of nucleolus decreased somewhat but remained greater than the baseline value (**Fig. 3c**).

To demonstrate tomographic imaging of a multicellular organism, we imaged the nematode *Caenorhabditis elegans*. We paralyzed the worms with 10 mM sodium azide in a nematode growth medium (NGM) buffer and imaged them in the same solution. We created overlapping tomograms and assembled the resulting data into a mosaic (**Fig. 3d** and **Supplementary Fig. 2** online). Several internal structures are visible, including a prominent pharynx and digestive tract.

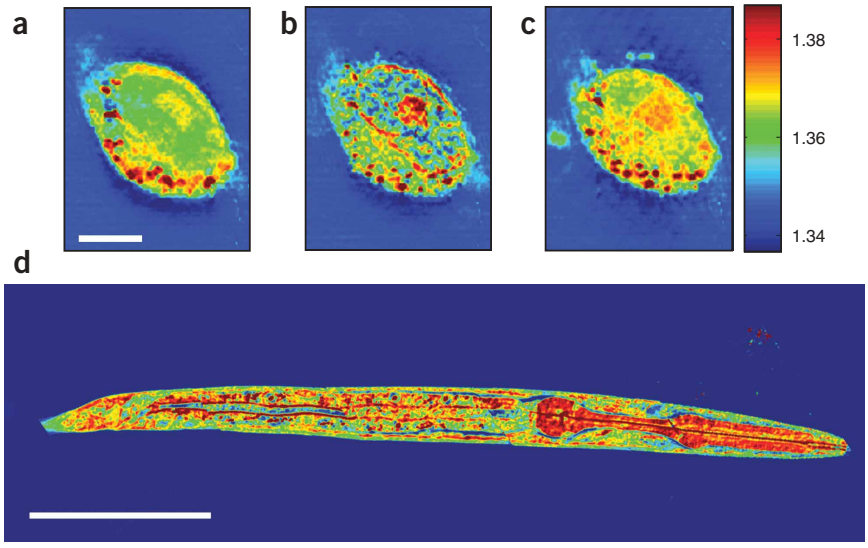

Figure 3 | Effects of acetic acid on a HeLa cell and imaging of *C. elegans*. (**a**–**c**) An *x*-*y* slice of tomogram from a HeLa cell in normal culture medium (**a**), after 3 min in medium containing 0.38% acetic acid (**b**), and 3 min after replacing the original medium (**c**). Scale bar, 10 μm. (**d**) Mosaic of *x*-*y* slices of index tomograms through *C. elegans*. Anterior is to the right. Scale bar, 50 μm. Color bar, refractive index at $\lambda = 633$ nm.

Finally, we explored the imaging of thick samples by obtaining refractive index tomograms from phantoms composed of polystyrene beads suspended in an optical adhesive. For these samples, the projection approximation is no longer valid, as evidenced by the severely distorted images of out-of-focus beads (**Supplementary Fig. 3** online). By varying the objective focus, however, it was possible to obtain an accurate tomogram at any depth in the sample (**Supplementary Figs. 3** and **4** online). A 3D tomogram of a thick sample can then be obtained via a mosaic of tomograms focused at different depths (see **Supplementary Methods**).

In summary, we developed a technique for quantitative refractive index tomography of living cells and tissues. The 3D structure mapped by tomographic phase microscopy can complement the images revealed by techniques such as hematoxylin and eosin staining. Refractive index data can be used to study light-scattering properties of cells and tissues, and characterize sample-induced aberrations in microscopy. Characterization and correction of such aberrations may be particularly important for modern superresolution techniques such as STED[14] and structured illumination[15].

Note: Supplementary information is available on the Nature Methods website.

ACKNOWLEDGMENTS

This work was funded by US National Institutes of Health (P41-RR02594-18) and Hamamatsu Corporation.

AUTHOR CONTRIBUTIONS

W.C. and C.F.-Y. conducted the experimental setup, data acquisition and data analysis; S.O. contributed to the experimental setup; N.L. contributed to 3D visualization; W.C., C.F.-Y., K.B., R.R.D. and M.S.F. wrote the manuscript; M.S.F. supervised the project.

COMPETING INTERESTS STATEMENT

The authors declare no competing financial interests.

Published online at http://www.nature.com/naturemethods
Reprints and permissions information is available online at http://npg.nature.com/reprintsandpermissions

1. Booth, M.J., Neil, M.A., Juskaitis, R. & Wilson, T. *Proc. Natl. Acad. Sci. USA* **99**, 5788–5792 (2002).
2. Kam, Z., Hanser, B., Gustafsson, M.G., Agard, D.A. & Sedat, J.W. *Proc. Natl. Acad. Sci. USA* **98**, 3790–3795 (2001).
3. Ross, K. *Phase Contrast and Interference Microscopy for Cell Biologists*. (Edward Arnold Publishers, London, 1967).
4. Rappaz, B. *et al. Opt. Express* **13**, 9361–9373 (2005).
5. Lue, N. *et al. Opt. Lett.* **31**, 2759–2761 (2006).
6. Dunn, G.A. & Zicha, D. *J. Cell Sci.* **108**, 1239–1249 (1995).
7. Park, Y.K., Popescu, G., Badizadegan, K., Dasari, R.R. & Feld, M.S. *Opt. Express* **14**, 8263–8268 (2006).
8. Lauer, V. *J. Microsc.* **205**, 165–176 (2002).
9. Charriere, F. *et al. Opt. Lett.* **31**, 178–180 (2006).
10. Fang-Yen, C. *et al. Opt. Lett.* **32**, 1572–1574 (2007).
11. Kak, A. & Slaney, M. *Principles of Computerized Tomographic Imaging*. (Academic Press, New York, 1999).
12. Brunsting, A. & Mullaney, P.F. *Biophys. J.* **14**, 439–453 (1974).
13. Ronne, M. *J. Dairy Sci.* **72**, 1363–1377 (1989).
14. Hell, S.W. *Nat. Biotechnol.* **21**, 1347–1355 (2003).
15. Gustafsson, M.G.L. *Proc. Natl. Acad. Sci. USA* **102**, 13081–13086 (2005).